Materials Science-Poland
Volume 44 Issue 2 · pp. 63–78 · DOI: 10.2478/msp-2026-0016

Materials Science-Poland

Carbon sequestration mechanisms and performance evolution of alkali-activated slag during the mixing process

Research Article

Chia-Jung Tsai[1,2,3], Chih-Wei Lu[4]*, Jun-Xiang Huang[1], Wen-Shinn Shyu[1,2], Jin-Chen Hsu[5]

[1] *Department of Civil Engineering, National Pingtung University of Science and Technology, Pingtung 912301, Taiwan, R.O.C.*
[2] *Center for Water Resources Education and Research, National Pingtung University of Science and Technology, Pingtung, 912301, Taiwan, R.O.C.*
[3] *Construction and Water Resources Engineering Service Center, Pingtung, 912301, Taiwan, R.O.C.*
[4] *Department of Civil and Construction Engineering, National Taiwan University of Science and Technology, Taipei 106335, Taiwan, R.O.C.*
[5] *Department of Mechanical Engineering, National Yunlin University of Science and Technology, Douliu 64002, Taiwan, R.O.C.*

Received 22 July 2026; Accepted 13 August 2026

Abstract: This study investigated the direct incorporation of carbon dioxide (CO_2) during the mixing of alkali-activated ground granulated blast furnace slag as an alternative to traditional post-hardening carbonation. CO_2 was introduced during the final 30 s of mixing. The effects of alkali content and carbonation on CO_2 uptake, compressive strength, water absorption, and microstructure were evaluated. The results showed that CO_2 uptake increased with alkali content and exposure duration, with a maximum uptake of approximately 1.9% after 300 s of continuous CO_2 exposure. The gravimetric and thermogravimetric measurements showed strong agreement, with an R^2 of 0.99. For the selected mortar mixtures, 30 s of CO_2 exposure resulted in a 15–25% increase in 28-day compressive strength compared with non-carbonated specimens. However, water absorption showed a slight reduction. The microstructural analysis indicated carbonate-rich precipitates in pore and interparticle regions. The results demonstrate that introducing CO_2 during alkali activation can promote *in situ* carbonate formation while improving the later-age mechanical performance of GGBFS-based alkali-activated materials.

Keywords: *Carbonation • Carbon reduction • CO_2 mineralization • Resource efficiency*

1. Introduction

Greenhouse gases, including carbon dioxide (CO_2), methane (CH_4), and nitrous oxide (N_2O), are among the primary drivers of global warming. Their increasing concentrations have significantly altered climate systems, making climate change one of the most critical global challenges. Among greenhouse gases, CO_2 is considered one of the main contributors to global warming due to its high emission volume and close association with industrial and construction activities. Therefore, technologies for CO_2 reduction, capture, and sequestration have emerged as important approaches for mitigating emissions and promoting sustainable development. Concrete, the most widely used construction material worldwide, contributes substantially to carbon emissions within the construction sector [1,2]. In particular, Portland cement, the primary binder in concrete, is recognized as a major contributor to global carbon emissions due to the energy-intensive manufacturing process and the large amount of CO_2 released during clinker production [3,4]. Therefore, integrating carbon reduction strategies and CO_2 capture/sequestration mechanisms into concrete systems to promote carbon circularity and sustainable engineering has become an important research focus in green materials science [5–7]. Alkali-activated materials (AAMs), particularly those based on ground granulated blast furnace slag (GGBFS), have been widely recognized as promising substitutes for ordinary Portland cement (OPC) due to their low carbon footprint, high durability, and effective utilization of industrial by-products [8–11]. These materials are formed through alkaline activation reactions

* *E-mail: cwlu@mail.ntust.edu.tw*

Open Access. © 2026 the author(s), published by Wroclaw University of Science and Technology
This work is licensed under the Creative Commons Attribution-NonCommercial-NoDerivs 4.0 License.

and typically produce amorphous to semi-crystalline gel structures, which lead to their excellent mechanical performance and long-term stability [12,13].

AAMs offer significant potential for carbon emission reduction compared with traditional cement systems [14,15] and have shown the ability to react with CO_2 to form stable carbonate phases [16], thereby providing dual functionality in carbon reduction and carbon sequestration within a single material system [17]. AAMs under CO_2 exposure conditions can achieve carbon sequestration through multiple complementary mechanisms. First, CO_2 dissolves in the pore solution to form carbonate (CO_3^{2-}) and bicarbonate (HCO_3^-) species [9]. These species subsequently react with dissolved Ca^{2+} ions within the matrix to form stable calcium carbonate ($CaCO_3$). This mineralization process effectively immobilizes CO_2 in solid form while simultaneously contributing to pore refinement and matrix densification [9–11]. As a result, carbonation reactions in AAMs can simultaneously enhance CO_2 sequestration capacity and modify the microstructural evolution of the binder system. Beyond these *in situ* carbonation mechanisms, CO_2-related chemistry can also be intentionally incorporated into AAM design strategies. Previous studies have explored the use of Na_2CO_3 as an alkali activator, utilizing carbonate-based alkaline environments to promote internal carbonate formation reactions while reducing the environmental issues related to traditional highly alkaline activators [15,18]. Furthermore, the direct incorporation of $CaCO_3$ as a filler or reactive component provides an external carbonate source that can refine pore structure and influence hydration or geopolymerization processes depending on the binder system [19]. Collectively, these approaches highlight the potential of integrating CO_2 chemistry into both the intrinsic reaction pathways and the mix design of AAMs, thereby enabling a synergistic framework for carbon reduction and carbon sequestration. Despite the growing interest in CO_2 mineralization in AAMs, most carbonation-based approaches have been investigated as a post-treatment process, in which hardened specimens are exposed to CO_2 after alkali activation and curing. This sequential approach separates alkali activation from carbonation and may limit the interaction between dissolved species released during activation and CO_2 at the early stage of material formation. Consequently, the potential for incorporating CO_2 directly during the fresh mixing and alkali-activation process, while simultaneously developing the binding matrix, remains insufficiently understood. Moreover, previous studies have largely evaluated CO_2 uptake, mechanical performance, or microstructural changes separately. The relationship between CO_2 incorporation during mixing, $CaCO_3$ formation, development of the C–(A)–S–H matrix, and the resulting changes in mechanical and transport-related properties has not been sufficiently established for CO_2-coupled alkali-activated GGBFS. In particular, the role of Ca-rich slag chemistry in promoting *in situ* carbonation and the extent to which the resulting carbonate phases contribute to pore filling and matrix densification require further clarification. A quantitative comparison between independent CO_2-uptake measurements and direct characterization of the resulting carbonate phases is also needed to strengthen the interpretation of the sequestration mechanism. Therefore, this study proposes a novel framework based on an alkali-activated slag (AAS) system, in which CO_2 is directly incorporated during the mixing process rather than treating carbonation as a post-hardening process. The primary objective was to clarify the influence of CO_2 on early-age gel formation, carbon sequestration behavior, associated reaction mechanisms, and to explain its relationship with the mechanical performance of hardened materials at later ages. This study employed a combination of mechanical testing and multiscale microstructural characterization techniques to systematically analyze structural evolution, gel formation behavior, and carbonate mineralization characteristics using Thermogravimetric analysis (TGA) and Scanning electron microscopy (SEM). Through this integrated approach, the study aims to provide a comprehensive understanding of how CO_2 participates in the hydration/activation environment and influences both the microstructural development and macroscopic performance of AAS systems.

2. Materials and methods

This study introduces a novel experimental design as a CO_2-coupled geopolymerization pathway (CCGP). Figure 1 illustrates the difference between the traditional method and the introduced method in this study. In contrast to traditional carbonation treatments applied after binder hardening, CO_2 was injected during the mixing stage, which enabled simultaneous carbonation and alkali activation of GGBFS.

The dissolved calcium species rapidly reacted with CO_2 to form nano-sized $CaCO_3$ particles, which acted as heterogeneous nucleation sites for C–(A)–S–H gel growth. This coupled reaction pathway resulted in a densified microstructure characterized by reduced porosity and enhanced particle packing.

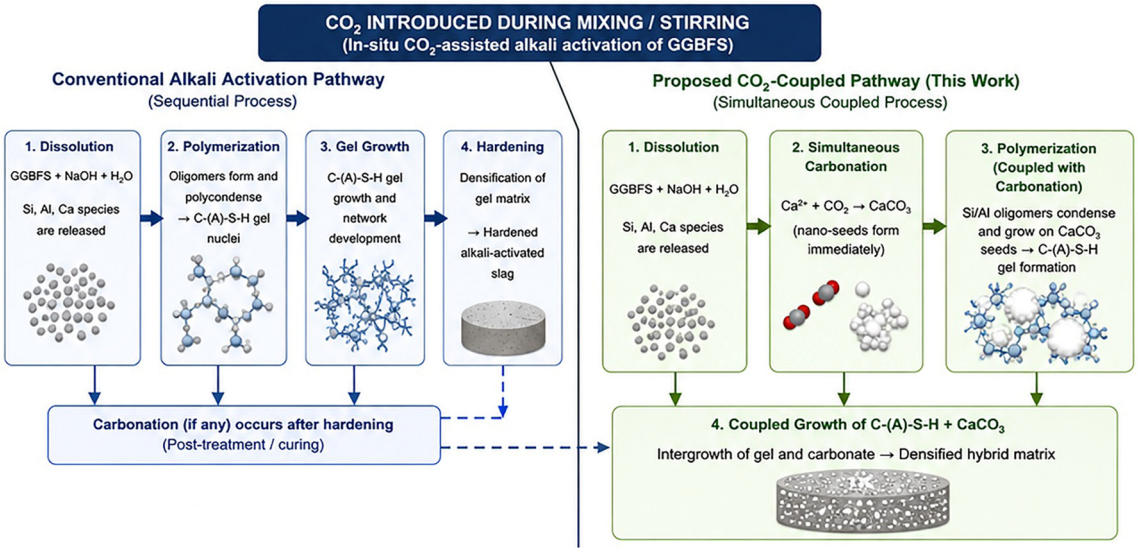


Figure 1. The CCGP method.

2.1 Materials

The materials used in this study include GGBFS, sodium hydroxide (NaOH), sodium silicate (Na_2SiO_3) solution, natural fine aggregates, and carbon dioxide (CO_2) gas.

2.1.1 Precursor material

GGBFS is a by-product of ironmaking in blast furnace processes. It is rapidly quenched with water to form an amorphous glassy structure, which reveals latent hydraulic reactivity. Its main chemical composition consists of CaO, SiO_2, Al_2O_3, and MgO, in which CaO and SiO_2 serve as the dominant phases that provide essential calcium and silicon sources for subsequent alkali-activation reactions. In this study, the GGBFS has a specific gravity of 2.90 g/cm^3 and a specific surface area of 564 m^2/kg. The activity index corresponds to Grade 120, in accordance with ASTM C989/C989M-25 "*Standard Specification for Slag Cement for Use in Concrete and Mortars*" [20]. The material was supplied by Jinyu Industrial Co, Ltd. Table 1 shows the chemical composition and physical properties of the material. The relatively high CaO content of the GGBFS is particularly relevant to the proposed CO_2-coupled alkali activation mechanism. Under alkaline conditions, calcium-containing phases in the slag can dissolve and release Ca^{2+} into the reaction environment. The availability of Ca^{2+} provides a favorable chemical pathway for the reaction with dissolved CO_2 and subsequent formation of $CaCO_3$. Therefore, the Ca-rich composition of the slag can be considered advantageous for *in situ* CO_2 mineralization. However, CaO content alone does not determine the carbonation capacity of the material, because Ca^{2+} availability also depends on the dissolution kinetics of the slag, the alkalinity of the activating solution, pore structure, and CO_2 transport. Therefore, the high CaO content should be regarded as a favorable chemical characteristic for carbonation rather than as an independent indicator of carbonation performance.

Chemical composition	Data	Physical analysis		Data
SiO_2%	34.58	Specific gravity (g/cm^3)		2.90
Al_2O_3%	14.28	Specific surface area (m^2/kg)		564
FeO%	0.50	Air content of mortar (volume)%		6.0
CaO%	42.75	Activity index (%)	7 days	95
MgO%	5.92		28 days	139
SO_3%	0.06			
Na_2O%	0.253			
K_2O%	0.432			
Other%	1.23			
Loss on ignition (LOI)%	0.28			

Table 1. Chemical composition and physical analysis of precursor materials.

2.1.2 Alkali activators

Sodium hydroxide (NaOH) with a purity of 95% was used as the primary alkali activator to provide a highly alkaline

environment, promoting the dissolution and depolymerization of the slag precursor. Sodium silicate (Na_2SiO_3) solution was employed as both a silica source and a supplementary activator, enabling adjustment of the SiO_2/Na_2O ratio in the activator solution. This ratio plays a critical role in controlling the formation and structural evolution of hydration and geopolymeric reaction products. The sodium silicate solution contained 32.2% SiO_2 and 13.18% Na_2O, with a Baume degree (°Bé) of 50.

2.1.3 CO_2

Carbon dioxide gas with a purity of approximately 99.9% was supplied from a high-pressure gas cylinder. The gas was injected into the reaction system during carbonation experiments to evaluate the carbon uptake behavior and sequestration capacity of the AAMs.

2.1.4 Fine aggregates

Natural fine aggregates were used in this study, with SiO_2 as the dominant constituent. The specific gravity and water absorption were 2.65 and approximately 1.2%, respectively. The particle size distribution (Figure 2) followed the standard requirements for fine aggregates, with a maximum particle size of 4.75 mm and a fineness modulus of 2.47. The particle-size distribution of the fine aggregate is an important factor in determining particle packing and the resulting pore structure of the mortar. A well-graded aggregate can improve packing efficiency by reducing the volume of interparticle voids. Consequently, it decreases the amount of paste required to fill the aggregate skeleton. This can influence water demand, porosity, water absorption, and ultimately compressive strength. Therefore, the aggregate grading was considered not only for compliance with the relevant specification but also to maintain a consistent particle-size distribution. This was necessary to minimize variations in packing and isolate the effects of alkali activation and CO_2 incorporation.

2.2 Experimental system

In this study, GGBFS was used as the precursor for AAS. The silica modulus (SiO_2/Na_2O) of the activator was fixed at 0.8, while the alkali content was selected as the experimental variable, ranging from 2 to 7% (i.e., 2, 3, 4, 5, 6, and 7%) to evaluate its influence on the carbon sequestration behavior and engineering performance of the material. In addition, a non-carbonated AAS specimen was prepared as the control group for comparison. The carbonated and non-carbonated specimens were indicated as AASS and AAS, respectively. To increase the contact efficiency and reaction extent between CO_2 and the alkali-activated gel system, the water-to-binder ratio was fixed at 0.6 to facilitate CO_2 diffusion and reaction within the paste. Considering the practical construction conditions and material workability, the mixing procedure was designed based on the minimum batching requirement of approximately 3 m^3 of concrete. The total mixing time was set to 90 s and divided into two stages according to different reaction environments. First, the mixture was mechanically mixed under vacuum conditions for 60 s to achieve a homogeneous dispersion state. Subsequently, CO_2 gas was injected into the mixing system, and mixing was continued for 30 s in a carbonation environment to simulate the rapid injection of CO_2 and the gel reaction process in practical engineering applications. The CO_2

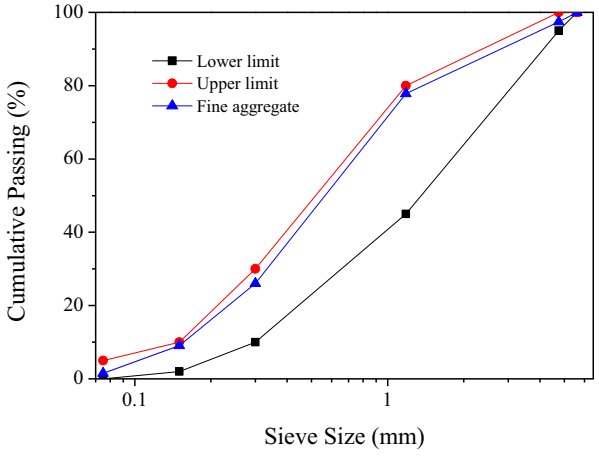


Figure 2. Particle size distribution curve of fine aggregate.

uptake capacity of each mix was quantified by measuring the mass difference between carbonated and non-carbonated specimens. This approach was used to evaluate the carbon sequestration potential under different mix proportions and limited reaction time (30 s).

In addition, TGA was employed to quantify carbonate formation and to verify the reliability of the mass-based CO_2 uptake estimation. These combined approaches further explained the carbonation mechanism in AAS systems and enabled identification of the optimal alkali content for subsequent mechanical and microstructural analyses. In the subsequent experimental phase, the influence of aggregate content on mechanical performance and carbonate filling was evaluated using slag-to-aggregate ratios of 1:1, 1:2, and 1:3. Compressive strength tests were applied to assess strength development behavior, while water absorption tests were performed to indirectly evaluate pore structure and material densification. Moreover, SEM was used to observe the microstructural morphology and the spatial distribution of reaction products, thereby indicating the influence of carbonation on internal structural evolution. Finally, by integrating macroscopic engineering properties with microscopic analysis results, the effects of alkali content on the carbonation mechanism of AAMs and their relationship with the overall material performance were systematically analyzed.

2.3 Experimental methods

2.3.1 Gravimetric evaluation of CO_2 sequestration capacity

The CO_2 sequestration capacity of the specimens was evaluated using a gravimetric method based on mass variation before and after carbonation. Immediately after mixing under vacuum conditions, the initial mass of each specimen (W_0) was measured as the baseline value and recorded. The specimens were subsequently exposed to a CO_2 atmosphere to promote carbonation reactions, during which CO_2 reacted with reactive components within the matrix to form carbonate products. After the carbonation process was completed, the specimens were removed, and their post-carbonation mass (W_1) was measured under the same conditions. The estimated CO_2 uptake was calculated from the relative mass increase between the pre- and post-carbonation states according to equation (1).

$$\text{Co}_2 \text{ uptake } (\%) = \frac{W_1 - W_0}{W_0} \times 100, \tag{1}$$

where W_0 is the mass of the specimen before carbonation, and W_1 is the mass of the specimen after carbonation.

2.3.2 TGA test method

TGA was employed to evaluate the mass change behavior of the materials during heating. This enables characterization of the thermal decomposition behavior of reaction products and quantification of carbonate content to estimate the CO_2 sequestration capacity of AAMs. TGA effectively distinguishes mass loss behaviors across various temperature ranges, including the dehydration of hydration products (such as C-(A)-S-H gel and bound water) and the thermal decomposition of carbonate phases (mainly $CaCO_3$). To remove the background influence of non-carbonate components, an uncarbonated specimen was used as a blank reference. The net CO_2 uptake was estimated from the difference in LOI between carbonated and uncarbonated specimens, as expressed in equation (2).

$$\text{Co}_2 \text{ uptake(wt.\%)} = \text{LOI}_{\text{carbonated}} - \text{LOI}_{\text{blank}}. \tag{2}$$

2.3.3 Microstructural analysis

This study employed SEM coupled with Energy dispersive X-ray spectroscopy (EDS) to investigate the microstructural evolution and elemental composition of AAMs under different alkali contents and carbonation conditions. The AAS mixtures were first mixed under vacuum conditions to minimize interference from atmospheric gases and moisture. CO_2 gas was then introduced directly into the mixing chamber during the designated carbonation period. This allowed CO_2 to interact with the freshly activated slag paste during mixing. After reaching the designated curing age, the specimens were placed in an oven at 110°C ± 5°C for 24 h to stop further reaction before sampling. SEM/EDS specimens with approximate dimensions of 10 × 10 × 5 mm were then prepared from the dried material for microstructural observation and elemental analysis. TGA specimens were similarly dried and subsequently ground into powder before thermal analysis.

SEM was used to observe surface morphology, pore structure, formation of reaction products, and the distribution of unreacted particles. In addition, SEM was used to evaluate the extent of alkali activation and the densification behavior of the microstructure. Observations at multiple magnifications were performed to compare microstructural variations before and after CO_2 exposure, including the development of C-(A)-S-H gel, precipitation of $CaCO_3$ crystals, and pore-filling phenomena. EDS analysis

was used to provide qualitative and semi-quantitative elemental characterization of localized regions, focusing on elements including Ca, Si, Al, Na, and C. The elemental composition data were used to identify changes in alkali-activation products and carbonate formation, thereby providing additional evidence for interpreting CO_2 sequestration mechanisms and carbonation effectiveness.

2.3.4 Compressive strength and water absorption tests

Compressive strength and water absorption tests were used following the standard ASTM C109/C109M-21 "Standard test method used to measure the compressive strength of hydraulic cement mortars" [21] and ASTM C642-21 "Standard Test Method for Density, Absorption, and Voids in Hardened Concrete" [22], respectively. Cubic specimens with dimensions of 50 × 50 × 50 mm were prepared, and three replicate specimens were tested for each mixture proportion at each designated curing age. Aggregate content was selected as the main experimental variable, and the mass ratios of binder to aggregate were designed as 1:1, 1:2, and 1:3. Different aggregate contents were employed to generate varying pore structures, thereby enabling evaluation of the influence of carbonation on the mechanical performance and pore compaction behavior of AAS materials.

2.4 Statistical analysis

Quantitative experimental results were obtained from replicate specimens for each experimental condition and are reported as the mean value ± standard deviation. The number of specimens used for each test was recorded separately according to the corresponding experimental procedure. Error bars in the figures represent the standard deviation of the replicate measurements. The coefficient of determination (R^2) was used to evaluate the strength of the linear relationship between the corresponding quantitative variables, including the relationship between water absorption and compressive strength and the agreement between the gravimetric and TGA-based CO_2 uptake measurements.

3. Results and discussion

3.1 Carbon sequestration efficiency of AAS

This study investigated the CO_2 uptake behavior of AAS under a CO_2 environment from three perspectives: time evolution, early-age reaction behavior, and long-term maximum adsorption capacity. First, the time-dependent characteristics of CO_2 fixation were analyzed by monitoring mass variation curves during mixing under a CO_2 atmosphere for specimens with different alkali contents, which revealed the overall reaction trends. Second, since the mixing procedure followed a standard 90 s protocol, consisting of 60 s of conventional mixing followed by 30 s of mixing under a CO_2 environment, particular focus was on the 30 s CO_2 exposure stage. This stage was used to evaluate the early-age CO_2 fixation capacity during practical mixing conditions and to identify the optimal reaction window for different alkali dosages. Finally, the maximum adsorption behavior of specimens with different alkali contents under continuous CO_2 exposure was analyzed to assess the long-term CO_2 sequestration capacity, cumulative uptake, and adsorption saturation behavior. This analysis further enabled evaluation of the influence of alkali content on the overall CO_2 fixation potential.

3.1.1 Evolution behavior of CO_2 during the mixing process of AAS paste

Figure 3 presents the mass variation curves of AAS with different alkali contents during the mixing process in a CO_2 environment, which reflect the CO_2 fixation behavior of the paste. The overall results indicate that CO_2 uptake increased continuously with mixing time. This suggests progressive reactions between dissolved CO_2 and reactive species in the system, including Ca^{2+}, silicate, and aluminate ions, leading to the gradual formation of carbonate-bearing products. In terms of time-dependent behavior, all mixtures showed a continuous increase in CO_2 fixation

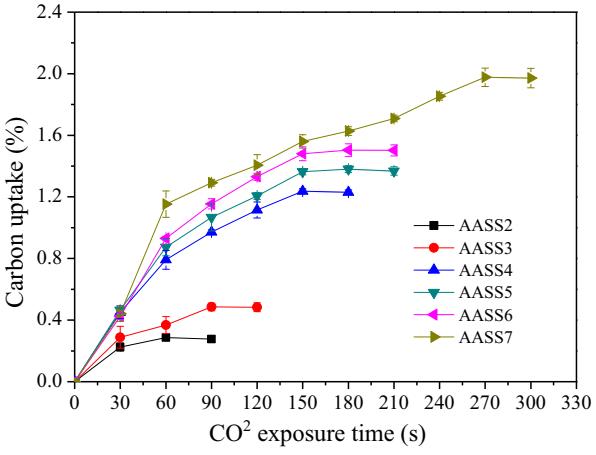


Figure 3. Relationship between CO_2 fixation amount and mixing time under different alkali equivalent conditions.

with increasing mixing time, demonstrating the kinetic nature of the carbonation process.

The results showed that as the alkali content increased, both the magnitude of mass change and the reaction rate increased simultaneously. This behavior is mainly related to the higher OH^- concentration in highly alkaline environments [23], which enhances slag dissolution and accelerates the release of Ca^{2+} and dissolved silicate species [24,25]. Consequently, the system more readily reaches a state of local supersaturation, promoting the formation of carbonate phases such as $CaCO_3$ [26]. Meanwhile, accelerated formation of C-(A)-S-H gel provided additional reactive interfaces, further facilitating continuous CO_2 uptake at the solid–liquid interface [27,28].

3.1.2 Early-stage reaction of AAS paste under CO_2 environment (30 s)

Figure 4 presents the CO_2 uptake behavior of AAS with different alkali contents and CO_2-exposed AAS paste (AASS) during the early stage (30 s). The AAS samples mixed under a sealed environment showed negligible mass variations, ranging from approximately 0.003 to 0.05%. Since no CO_2 exposure occurs throughout the test, these minor fluctuations were attributed to instrumental noise and transient physical effects, such as fluid redistribution, particle rearrangement, and short-term variations in sensor response, rather than to chemically induced mass changes.

In contrast, AASS specimens showed significant differences in early-stage CO_2 uptake depending on alkali content. Specimens with low alkali contents (2–3%) revealed CO_2 uptake values of 0.22–0.29%, indicating limited early reactivity. This was mainly related to insufficient slag dissolution and restricted ion release under low-alkaline conditions, which delayed the formation of C-(A)-S-H gel and the onset of carbonate reactions.

When the alkali content was increased to above 4%, CO_2 uptake increased significantly to about 0.42–0.46% and gradually stabilized, indicating that the system entered a more effective reaction regime. At this stage, the higher alkalinity enhanced the slag dissolution and accelerated the release of Ca^{2+} and dissolved silicate species, promoting local supersaturation. This facilitated the formation of C-(A)-S-H gel and carbonate phases, thereby shifting the CO_2 fixation behavior from a kinetically limited regime to a more stable reaction regime.

3.1.3 Maximum carbon sequestration capacity of AAS under CO_2 mixing conditions with different alkali contents

The results showed clear differences among specimens with varying alkali contents in the maximum CO_2 uptake behavior under continuous CO_2 exposure. Specimens with low alkali contents (2–3%) showed relatively limited maximum CO_2 uptake capacities of 0.28 and 0.49%, respectively, indicating poor long-term carbon sequestration performance. Increasing the alkali content to 4% markedly increased CO_2 uptake capacity over exposure time. Among all mixtures, the AASS7 specimen (7% alkali content) revealed the best performance. The sample reached a total CO_2 uptake of approximately 1.9% after approximately 300 s of continuous carbonation (Figure 5). The results suggested that a highly alkaline environment effectively enhanced slag dissolution kinetics and increased the supply of reactive ionic species. This enabled the system to sustain both carbonate precipitation and gel formation under prolonged CO_2 exposure conditions, thereby improving overall carbon sequestration capacity.

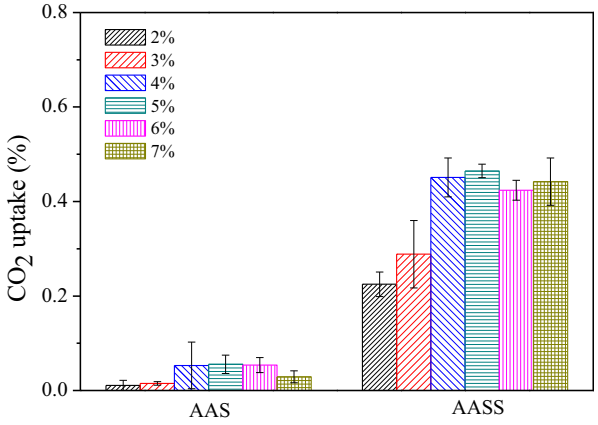


Figure 4. Comparison of CO_2 uptake after 30 s exposure to a CO_2 environment.

3.2 Quantitative evaluation of thermal analysis and CO_2 fixation mechanism in AAS

3.2.1 Quantitative evaluation of thermal analysis

It is important to distinguish between the 30 s and maximum CO_2-exposure conditions used in this study. The 30 s condition represents the practical CO_2 injection period incorporated into the 90 s mixing procedure and was therefore used to evaluate early-stage CO_2 fixation under a realistic mixing condition. In contrast, the maximum CO_2 uptake was determined under continuous CO_2 exposure for approximately 300 s to investigate the cumulative carbonation capacity of the material beyond the practical mixing period. Therefore, the higher CO_2 uptake observed under the maximum-exposure condition is expected because the system was allowed substantially more time for slag dissolution, CO_2 dissolution, Ca^{2+} release, and carbonate precipitation. The two conditions were used to evaluate different aspects of the carbonation process and should not be interpreted as equivalent exposure conditions. Figures 6 and 7 illustrate the TGA and derivative thermogravimetric (DTG) curves of AAS with different alkali contents under various CO_2 exposure conditions. The TGA results indicated continuous mass loss during the heating process in all specimens. However, the overall mass reduction rate did not show any significant changes related to either alkali content or CO_2 exposure conditions. Further interpretation of the DTG curves revealed a clearer identification of characteristic thermal events in different temperature ranges. Distinct peaks were observed at approximately 100°C, 600°C, 750°C, and 800°C, which are related to different dehydration and decomposition processes in the alkali-activated matrix and its carbonation products.

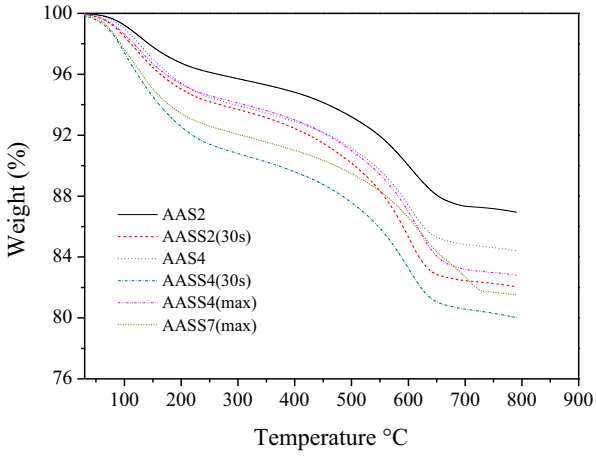


Figure 6. TGA curves of AAS under different CO_2 exposure durations.

In the low-temperature range (approximately 60–160°C), the observed mass loss was primarily associated with the evaporation of physically bound water and the dehydration of reaction products [9,16]. This mass loss is mainly attributed to the release of structural water from C-(A)-S-H gel and other hydration/activation products, resulting in the initial dehydration peak. The DTG curves mainly reflected continued decomposition of hydration products within the intermediate temperature range (approximately 300–600°C). In AAS systems, this region is generally associated with progressive dehydration of C-(A)-S-H gel and other metastable phases, producing a broader and more gradual mass loss profile [23]. In addition, if calcium hydroxide-containing phases are

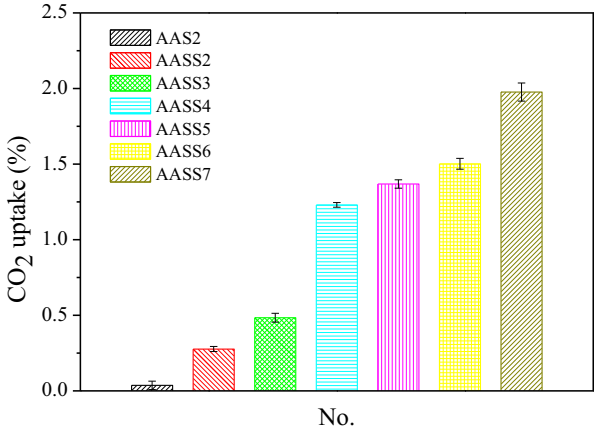


Figure 5. Comparison of maximum CO_2 fixation capacities under continuous CO_2 exposure at different alkali equivalents.

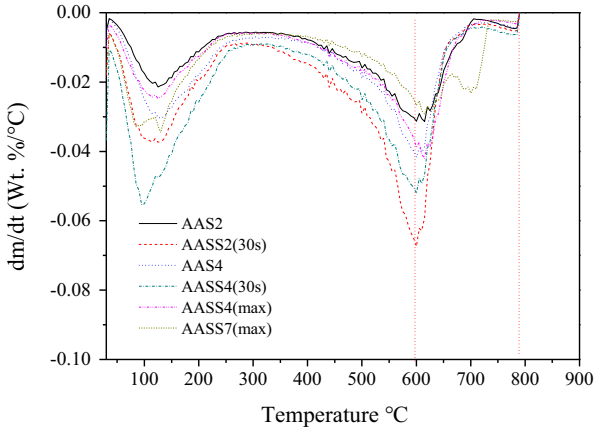


Figure 7. DTG curves of AAS under different CO_2 exposure durations.

present, dehydroxylation reactions may occur within approximately 425–480°C; however, the contribution of portlandite in AAS systems is typically limited compared with OPC systems [16,23].

At higher temperatures (approximately 600–800°C), noticeable DTG peaks were linked with the thermal decomposition of carbonate phases formed during carbonation. In this temperature range, calcium carbonate ($CaCO_3$) undergoes decarbonation, releasing CO_2 ($CaCO_3 \rightarrow CaO + CO_2$) [29] and generating characteristic mass loss peaks that are commonly used to quantify carbonate content in alkali-activated systems. The presence and intensity of these peaks provide important evidence for carbonate formation and can be used to evaluate the effectiveness of CO_2 sequestration under different alkali contents and carbonation conditions. Furthermore, variations in peak position and intensity may reflect differences in carbonate type, crystallinity, and degree of carbonation within the matrix. The mass loss within the 600°C–800°C range was extracted and converted into CO_2 content (%) using the corresponding calculation method (Figure 6).

Figure 8 shows the mass loss related to carbonate decomposition at a temperature of 600°C–800°C. The results demonstrated that AAS paste has CO_2 sequestration capability and that CO_2 uptake increased with increasing alkali concentration and exposure duration. The AAS2 and AAS4 showed nearly negligible CO_2 content (approximately 0%). In contrast, AASS2 (30 s), AASS4 (30 s), AASS4 (max), and AASS7 (max) showed values of 0.21, 0.48, 1.06, and 1.96%, respectively.

3.2.2 Ca^{2+}-dominated carbonate formation mechanism and alkali content effect

The thermal decomposition behavior observed in the TGA/DTG results revealed that the carbon sequestration

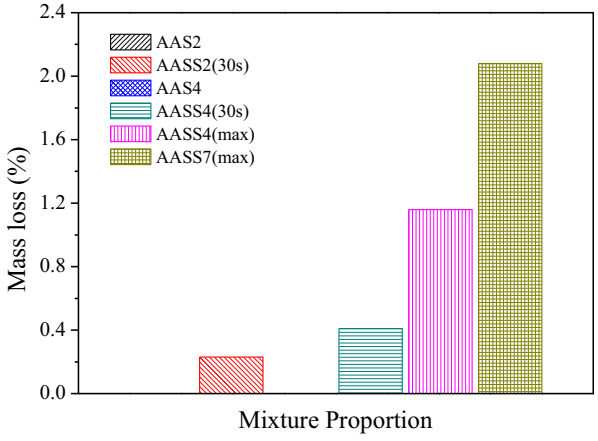


Figure 8. Mass loss associated with carbonate decomposition (600–800°C).

behavior of AAS is mainly controlled by a Ca^{2+}-mediated carbonate formation mechanism, in which the C-(A)-S-H gel structure plays an important role in regulating ion transport and controlling reaction interfaces. GGBFS mainly consists of Ca, Si, Al, and Mg, which are mostly present in oxide forms such as CaO, SiO_2, Al_2O_3, and MgO. Under alkaline activation conditions, Na^+ and OH^- increase dissolution and depolymerization of the amorphous slag phase by breaking Si–O–Si and Si–O–Al bonds, resulting in the release of reactive ionic species, including Ca^{2+}, Mg^{2+}, silicate, and aluminate species. These dissolved species subsequently participate in polymerization and precipitation reactions, leading to the formation of a C-(A)-S-H-dominated gel network while simultaneously increasing the Ca^{2+} concentration within the pore solution, which provides an essential reactive source for subsequent carbonation reactions [9,30–32]. The results revealed that under CO_2 exposure, carbonation was controlled by ionic reactions occurring in the pore solution. Therefore, Ca^{2+} serves as the dominant reactive species. Dissolved Ca^{2+} reacted with carbonate species generated from dissolved CO_2 to form stable $CaCO_3$ precipitates, which represent the major pathway for carbon fixation [33]. Although Mg^{2+} might also participate in carbonation reactions through the formation of Mg-containing carbonate phases ($MgCO_3$), its contribution to overall carbon sequestration is generally limited because of slower reaction kinetics and the lower extent of carbonate formation. Therefore, specimens with higher alkali contents show enhanced CO_2 uptake capacity due to accelerated slag dissolution and greater availability of dissolved Ca^{2+} for carbonation reactions. In contrast, Si and Al primarily contribute to the formation of the C–(A)–S–H framework rather than directly participating in carbonate formation. However, they indirectly influence carbonation behavior by regulating pore structure, ion transport pathways, and reaction kinetics.

Furthermore, correlation analysis between the mass-balance method and CO_2 contents derived from TGA demonstrated an approximately linear relationship with a coefficient of determination (R^2) of 0.99, indicating excellent agreement between the two quantification approaches (Figure 9). These results confirm that the mass-based method provided a reliable and reproducible approach for evaluating CO_2 uptake in AAS systems. In addition, this strong agreement supports that carbonate formation by Ca^{2+}-driven mineralization governs the overall carbonation behavior of the system.

3.3 Strength development and microstructural evolution

3.3.1 Compressive strength

Figure 10 presents the compressive strength results of carbonated AAS systems (alkali dosage of 4%) with different slag-to-aggregate ratios (1:1, 1:2, and 1:3). The results indicated the highest compressive strength in specimens with a slag-to-aggregate ratio of 1:2. However, the 1:1 and 1:3 mixtures showed comparatively lower mechanical performance. The lower strength observed in the 1:1 mixture is due to the relatively high binder content, where strength development is mainly controlled by the gel matrix and might be more sensitive to shrinkage, pore formation, or matrix heterogeneity.

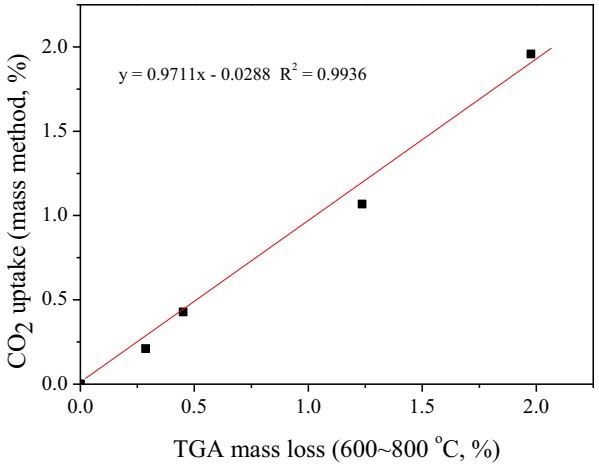


Figure 9. Relationship between the gravimetric method and the $CaCO_3$ decomposition-related mass loss.

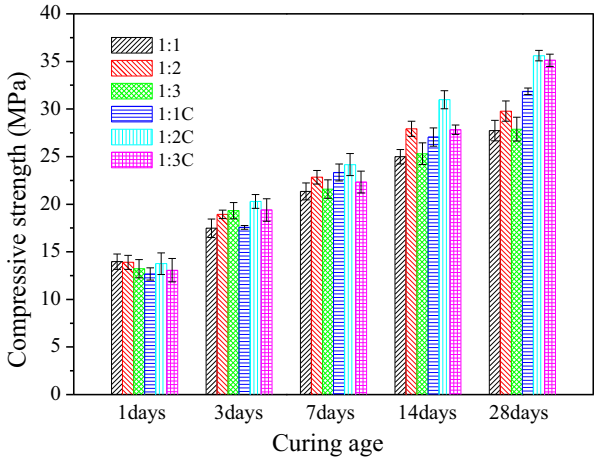


Figure 10. Effect of carbonation on the compressive strength of AAS mortar with different aggregate ratios.

In contrast, the 1:3 mixture contained a higher aggregate fraction, which reduced the continuity of the binding matrix and limited effective stress transfer within the composite system, while decreasing the overall mechanical performance. The 1:2 ratio appeared to provide a more balanced relationship between binder matrix formation and aggregate framework support, resulting in improved load transfer efficiency and enhanced strength development.

Under similar mixture proportions, after short-term CO_2 exposure (30 s), all specimens showed a slight reduction in compressive strength at 1 day of curing, about 1–9%. This behavior might be due to the rapid carbonation reaction consuming Ca^{2+} in the pore solution at early ages. This reaction can temporarily interfere with initial hydration and geopolymerization processes. However, with increasing curing age, compressive strength gradually recovered and showed a clear increasing trend. At 28 days of curing, all carbonated groups indicated an overall increase in compressive strength of approximately 15–25% compared with the non-carbonated specimens. This suggested that short-term CO_2 exposure could not hinder long-term strength development and might enhance compressive strength. The improvement is mainly attributed to the formation of calcium carbonate precipitates, which act as pore-filling products, refining the microstructure and increasing matrix densification. The results show enhanced compressive strength development under CO_2 curing [34,35]. This suggests a beneficial role of carbonation reactions in improving the performance of alkali-activated systems through microstructural densification. Furthermore, comparable strength of the 1:3 mixture

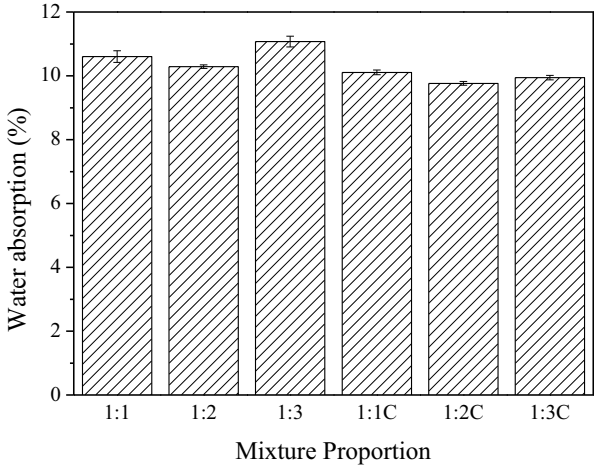


Figure 11. Effect of carbonation on water absorption of AAS mortar with different aggregate ratios.

with the 1:2 mixture at 28 days suggests that continued hydration and carbonation reactions partially compensate for the lower initial gel content and reduced matrix continuity in mixtures with higher aggregate fractions.

3.3.2 Water absorption

Figure 11 shows the water absorption results of AAMs under different mix proportions and CO_2 exposure conditions. The water absorption values of all specimens range from approximately 9.8 to 11%, with relatively minor variations among groups. This indicated that both aggregate ratio and short-term CO_2 exposure have a limited influence on the overall water absorption behavior. For the non-carbonated specimens, the 1:3 mix showed the highest water absorption (approximately 11%), which can be attributed to the increased porosity and reduced continuity of the binding matrix associated with higher aggregate content. In contrast, the 1:2 mix indicated relatively lower water absorption, suggesting a more compact pore structure and improved matrix packing. For the CO_2exposed specimens (1:1 C, 1:2 C, and 1:3 C), the water absorption values were slightly lower than their corresponding non-carbonated groups. This trend suggested that carbonation might promote the formation of $CaCO_3$ precipitates, which partially fill capillary pores and contribute to microstructural refinement, thereby reducing water uptake capacity. Kim et al. [36] reported that reductions in porosity and pore size due to carbonate formation led to slightly lower water absorption [36]. Although their study was conducted on Portland cement paste rather than AAS, the observed relationship between carbonation and pore-structure modification provides supporting evidence for the pore-filling interpretation proposed in the present study. Hwalla et al. [37] stated that water absorption decreased with increasing carbonation-curing duration and pressure. Their results indicated that carbonation conditions can influence the transport-related properties of AAS materials [37]. In addition, the small error bars across all groups indicated acceptable experimental repeatability and stability. Overall, short-term CO_2 exposure leads to a slight reduction in water absorption, suggesting a limited but measurable densification effect induced by carbonation in AAMs.

The correlation between water absorption and compressive strength was further analyzed. The results indicated a clear linear relationship between the two parameters, with a coefficient of determination (R^2) of 0.81, which showed a moderate-to-strong correlation between water absorption and compressive strength (Figure 12). The overall trend showed that higher compressive strength resulted in lower water absorption.

The findings suggested that carbonation-induced $CaCO_3$ formation reduced water transport pathways and enhanced mechanical performance simultaneously through pore filling and microstructural densification. This reflects a coupled relationship between moisture transport behavior and strength development in AAM systems.

3.3.3 Microstructural analysis

Figure 13 shows the SEM observations of AAS mortars under different carbonation conditions. Image (a) shows the uncarbonated specimen at 500× magnification, where localized microcracks and relatively loose interfacial regions can be observed, particularly around aggregate particles. In contrast, image (b) illustrates the carbonated specimen, in which granular precipitates are clearly

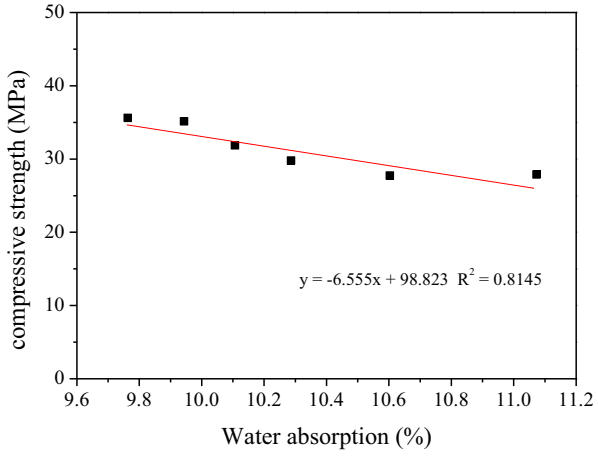


Figure 12. Relationship curve between water absorption and compressive strength.

distributed within interparticle voids and pore regions. At a higher magnification of 3,000× (image c), numerous white precipitates are observed along the particle interfaces and within the pore spaces, indicating pronounced precipitation and pore-filling characteristics. EDS analysis revealed that these regions are mainly enriched in Ca, C, and O, with dominant Ca and O signals, suggesting that the precipitates are likely associated with carbonate-rich phases, predominantly $CaCO_3$. The detected Si signal might originate from the surrounding slag matrix or adjacent aggregate particles. Wang et al. [38] demonstrated that carbonation can substantially modify the multiscale pore structure of AAS, while the extent of the modification depends on the characteristics of the slag and the carbonation conditions [38]. The comparison between Figure 13(a, b) provides qualitative evidence of carbonation-induced modification of the interfacial transition zone (ITZ). In the uncarbonated specimen, the ITZ appears relatively open, with localized microcracks around the aggregate particles. After carbonation, the observed precipitates occupy interparticle voids and regions adjacent to the aggregate surfaces, indicating local filling of the interfacial pores and partial closure of microcracks. This indicates that carbonation modifies and densifies the ITZ through carbonate precipitation. This microstructural change is also consistent with the reduction in water absorption and improvement in compressive strength observed after carbonation.

4. Limitations

Although the proposed framework indicated a promising route toward carbon-negative AAMs, several inherent limitations must be acknowledged. The present study did not quantitatively evaluate the fresh-state workability of the mixtures. Therefore, the influence of direct CO_2 introduction during mixing on workability cannot be conclusively established. Moreover, the gravimetric and TGA/DTG methods provide quantitative evidence of CO_2-associated

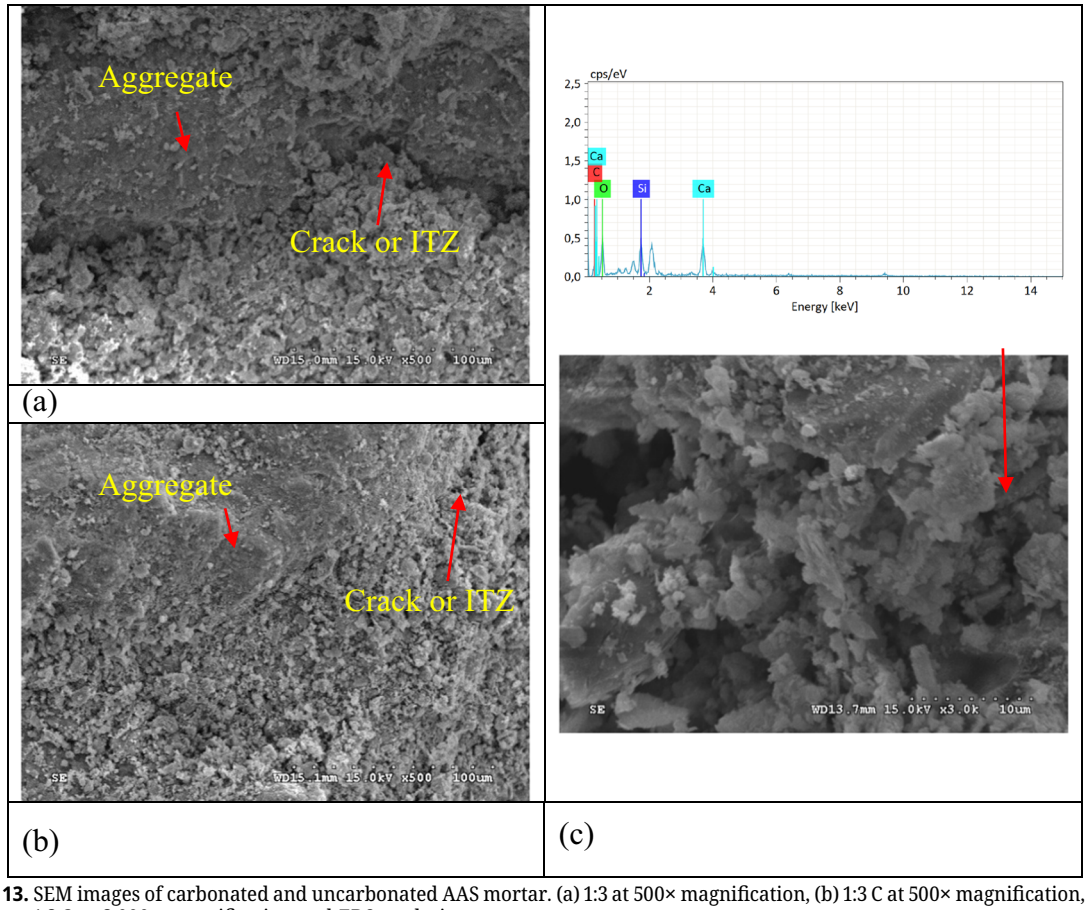


Figure 13. SEM images of carbonated and uncarbonated AAS mortar. (a) 1:3 at 500× magnification, (b) 1:3 C at 500× magnification, and (c) 1:3 C at 3,000× magnification and EDS analysis.

mass uptake and carbonate formation, but they do not independently establish the spatial penetration profile of CO_2 within the specimens. In addition, the experiments were conducted at laboratory scale and over the specified curing and exposure periods. Consequently, the long-term durability and field-scale performance of the CO_2-coupled AAM require further investigation. Although the results showed CO_2 incorporation and associated improvements in material performance, a complete life-cycle carbon balance was not performed. Therefore, the environmental significance of the process should not be interpreted as demonstrating net carbon negativity without accounting for the emissions associated with raw materials, activator production, CO_2 supply, energy consumption, and processing.

5. Conclusion

This study investigated the incorporation of CO_2 during the mixing and alkali activation of GGBFS and evaluated its effects on CO_2 uptake, mechanical performance, water absorption, and microstructural characteristics. The findings are as follows:

1. CO_2 uptake was strongly dependent on alkali content and exposure duration. Under the practical 30 s CO_2-mixing condition, increasing the alkali content promoted CO_2 uptake, with values increasing from approximately 0.22–0.29% at 2–3% alkali content to approximately 0.42–0.46% at alkali contents above 4%. Under continuous exposure, the 7% alkali mixture reached a maximum CO_2 uptake of approximately 1.9% after about 300 s.
2. The carbonation response was associated with Ca-rich slag chemistry and carbonate formation. The high CaO content of the GGBFS provided a favorable source of Ca^{2+} for carbonate precipitation under alkaline conditions. TGA/DTG identified carbonate-associated decomposition in the 600–800°C range. Moreover, SEM/EDS detected Ca-, C-, and O-rich precipitates in pore and interparticle regions.
3. The two CO_2-uptake quantification approaches showed strong agreement. The gravimetric mass-difference method and the TGA-based estimation of carbonate-associated CO_2 showed a coefficient of determination of 0.99. This agreement supported the reliability of the measured CO_2 uptake within the scope of the experimental procedure.
4. Short-term CO_2 exposure influenced the strength development in a time-dependent manner. A slight reduction of approximately 1–9% in compressive strength was observed at 1 day after 30 s of CO_2 exposure. However, the carbonated specimens showed approximately 15–25% higher compressive strength at 28 days compared to the corresponding non-carbonated specimens. Among the investigated aggregate ratios, the 1:2 mixture provided the most balanced combination of binder continuity and aggregate support.
5. Water absorption showed a slight reduction after CO_2 exposure. The measured values were approximately 9.8–11%, and the carbonated specimens generally indicated lower water absorption compared to non-carbonated mixtures.
6. The proposed CO_2-coupled alkali activation approach shows the potential for integrating CO_2 mineralization with material performance development. The results indicated that introducing CO_2 during the early mixing stage can promote carbonate formation while maintaining and, at later ages, improving the mechanical performance of AAS.

Overall, the proposed CO_2-assisted alkali activation approach offers a promising route toward carbon-negative AAMs.

Acknowledgments

The authors gratefully acknowledge the support and assistance provided by the Precision Instruments Center of the NPUST (Scanning Electron Microscope, SEM).

Funding information

This work was supported by a cooperative project between the National Pingtung University of Science and Technology (NPUST), National Yunlin University of Science and Technology (NYUST), and National Taiwan University of Science and Technology (NTUST) under Grant number [NPUST-NYUST-NTUST-115-01].

Author contributions

Chia-Jung Tsai: Writing – original draft, Visualization, Supervision, Methodology, Conceptualization. Chih-Wei Lu: Writing – review & editing, Visualization, Investigation, Formal analysis. Jun-Xiang Huang and Wen-Shinn Shyu: Visualization, Methodology, Investigation, Data curation, Jin-Chen Hsue: Writing – review & editing and Visualization.

Conflict of interest statement

The authors declare that they have no known competing financial interests or personal relationships that could

have appeared to influence the work reported in this manuscript.

Informed consent

Informed consent was obtained from all individual participants included in the study.

Ethical approval

This article does not contain any studies with human participants or animals.

Data availability statement

The data supporting the findings of this study are available within the manuscript.

References

[1] Lippiatt, N., Ling, T.-C., Pan, S.-Y., Towards carbon-neutral construction materials: Carbonation of cement-based materials and the future perspective, J. Build. Eng., 2020, 28: 101062. doi: https://doi.org/https://doi.org/10.1016/j.jobe.2019.101062

[2] Andrew, R. M., Global CO_2 emissions from cement production, 1928–2018, Earth Syst. Sci. Data, 2019, 11(4): 1675–1710. doi: https://doi.org/10.5194/essd-11-1675-2019

[3] Supriya, Chaudhury, R., Sharma, U., Thapliyal, P.C., Singh, L.P., Low-CO_2 emission strategies to achieve net zero target in cement sector, J. Clean. Prod., 2023, 417: 137466. doi: https://doi.org/https://doi.org/10.1016/j.jclepro.2023.137466

[4] Wu, S., Shao, Z., Andrew, R. M., Bing, L., Wang, J., Niu, L., et al., Global CO_2 uptake by cement materials accounts 1930–2023, Sci. Data, 2024, 11(1): 1409. doi: https://doi.org/10.1038/s41597-024-04234-8

[5] Habert, G., Miller, S. A., John, V. M., Provis, J. L., Favier, A., Horvath, A., et al., Environmental impacts and decarbonization strategies in the cement and concrete industries, Nat. Rev. Earth Environ., 2020, 1(11): 559–573. doi: https://doi.org/10.1038/s43017-020-0093-3

[6] Han, S., Kim, J. H., Singh, R. K., & Shah, S. P., CO_2 utilization for cementitious materials - A review, KSCE J. Civ. Eng., 2025, 29(4): 100227. doi: https://doi.org/https://doi.org/10.1016/j.kscej.2025.100227

[7] Al Salaheen, M., Alaloul, W. S., Alzubi, K. M., Malkawi, A. b. A., Musarat, M. A., Advancing waste-based construction materials through carbon dioxide curing: A comprehensive review, Results Eng., 2023, 20: 101591. doi: https://doi.org/https://doi.org/10.1016/j.rineng.2023.101591

[8] Charitha, V., Athira, G., Bahurudeen, A., Shekhar, S., Carbonation of alkali activated binders and comparison with the performance of ordinary Portland cement and blended cement binders, J. Build. Eng., 2022, 53: 104513. doi: https://doi.org/https://doi.org/10.1016/j.jobe.2022.104513

[9] Akturk, B., Abolfathi, M., Ulukaya, S., Kizilkanat, A. B., Hooper, T. J. N., Gu, L., et al., Hydration kinetics and performance of sodium carbonate-activated slag-based systems containing reactive MgO and metakaolin under carbonation, Cem. Concr. Compos., 2022, 132, 104617. doi: https://doi.org/https://doi.org/10.1016/j.cemconcomp.2022.104617

[10] Provis, J.L., Palomo, A., Shi, C., Advances in understanding alkali-activated materials, Cem. Concr. Res., 2015, 78: 110–125. doi: https://doi.org/https://doi.org/10.1016/j.cemconres.2015.04.013

[11] Puertas, F., Palacios, M., Vázquez, T., Carbonation process of alkali-activated slag mortars [Article], J. Mater. Sci., 2006, 41(10): 3071–3082. doi: https://doi.org/10.1007/s10853-005-1821-2

[12] Davidovits, J., Geopolymers, J. Therm. Anal., 1991, 37(8): 1633–1656. doi: https://doi.org/10.1007/BF01912193

[13] Lu, G., Wang, K., Theoretical and experimental study on shear behavior of fresh mortar, Cem. Concr. Compos., 2011, 33(2): 319–327. doi: https://doi.org/https://doi.org/10.1016/j.cemconcomp.2010.09.002

[14] Tsai, C.-J., Wu, B.-W., Hua, C.-Y., Wu, Y.-H., Lin, W.-T., Influence of alkali equivalent and aggregate type on the volumetric behavior of alkali-activated slag mortar during plastic and hardened phases, Mater. Today Adv., 2026, 29: 100716. doi: https://doi.org/https://doi.org/10.1016/j.mtadv.2026.100716

[15] Zhang, X., Long, K., Liu, W., Li, L., Long, W.-J., Carbonation and Chloride Ions' Penetration of Alkali-Activated Materials: A Review, Molecules, 2020, 25(21): 5074

[16] Bernal, S. A., de Gutierrez, R. M., Provis, J. L., Rose, V., Effect of silicate modulus and metakaolin incorporation on the carbonation of alkali silicate-activated slags, Cem. Concr. Res., 2010, 40(6): 898–907. doi: https://doi.org/https://doi.org/10.1016/j.cemconres.2010.02.003

[17] Lamaa, G. A.-O., Duarte, A. P. C., Silva, R. A.-O., de Brito, J. A.-O., Carbonation of Alkali-Activated

Materials: A Review, Materials, 2023. doi: https://doi.org/https://doi.org/10.3390/ma16083086

[18] Jeon, D., Jun, Y., Jeong, Y., Oh, J. E., Microstructural and strength improvements through the use of Na_2CO_3 in a cementless Ca(OH)2-activated Class F fly ash system, Cem. Concr. Res., 2015, 67, 215–225. doi: https://doi.org/https://doi.org/10.1016/j.cemconres.2014.10.001

[19] Velandia, D. F., Lynsdale, C. J., Provis, J. L., Ramirez, F., Gomez, A. C., Evaluation of activated high volume fly ash systems using Na_2SO_4, lime and quicklime in mortars with high loss on ignition fly ashes, Constr. Build. Mater., 2016, 128: 248–255. doi: https://doi.org/https://doi.org/10.1016/j.conbuildmat.2016.10.076

[20] ASTM, I., ASTM C989/C989M-25: Standard specification for slag cement for use in concrete and mortars, West Conshohocken, PA: ASTM International, 2025

[21] ASTM, I., ASTM C109/C109M-21: Standard Test Method for Compressive Strength of Hydraulic Cement Mortars (Using 2-in. or [50 mm] Cube Specimens), West Conshohocken, PA: ASTM International, 2024

[22] ASTM, I., ASTM C642-21: Standard test method for density, absorption, and voids in hardened concrete, West Conshohocken, 104617, PA: ASTM International, 2022

[23] Hidalgo, A., Domingo, C., Garcia, C., Petit, S., Andrade, C., & Alonso, C., Microstructural changes induced in Portland cement-based materials due to natural and supercritical carbonation, J. Mater. Sci., 2008, 43(9): 3101–3111. doi: https://doi.org/10.1007/s10853-008-2521-5

[24] García-Lodeiro, I., Palomo, A., Fernández-Jiménez, A., An overview of the chemistry of alkali-activated cement-based materials, Cem. Concr. Res., 2011, 41(9): 923–931

[25] Provis, J. L., Alkali-activated materials, Cem. Concr. Res., 2018, 114: 40–48

[26] Li, J., Wu, S., Huang, Y., Li, Z., Li, J., Shi, Y., Carbonation performance and environmental assessment of alkali-activated slag-fly ash-steel slag mortars: precursor composition effects revealed by quantitative carbonate zoning, Environ. Res., 2026, 288: 123252. doi: https://doi.org/https://doi.org/10.1016/j.envres.2025.123252

[27] Bernal, S. A., Provis, J. L., Walkley, B., Gel nanostructure in alkali-activated materials, Cem. Concr. Res., 2011, 41(7): 711–720

[28] Provis, J.L., van Deventer, J.S.J, Alkali Activated Materials: State-of-the-Art Report, RILEM TC 224-AAM. Springer, 2014

[29] Popescu, M.-A., Isopescu, R., Matei, C., Fagarasan, G., Valentin, P., Thermal decomposition of calcium carbonate polymorphs precipitated in the presence of ammonia and alkylamines, Adv. Powder Technol., 2014, 25: 500–507. doi: https://doi.org/10.1016/j.apt.2013.08.003

[30] Adesina, A., Early-age *in-situ* chemical composition evolution of alkali-activated slag under different activator systems, Mater., 2026, 11: 101997. doi: https://doi.org/https://doi.org/10.1016/j.nxmate.2026.101997

[31] John, S. K., Nadir, Y., Girija, K., Effect of source materials, additives on the mechanical properties and durability of fly ash and fly ash-slag geopolymer mortar: A review, Constr. Build. Mater., 2021, 280: 122443. doi: https://doi.org/https://doi.org/10.1016/j.conbuildmat.2021.122443

[32] Nguyen, T. N., Phung, Q. T., Frederickx, L., Jacques, D., Dauzeres, A., Elsen, J., et al., Microstructural evolution and its impact on the mechanical strength of typical alkali-activated slag subjected to accelerated carbonation, Dev. Built Environ., 2024, 19: 100519. doi: https://doi.org/https://doi.org/10.1016/j.dibe.2024.100519

[33] Ashraf, W., Carbonation of cement-based materials: Challenges and opportunities, Constr. Build. Mater., 2016, 120: 558–570. doi: https://doi.org/https://doi.org/10.1016/j.conbuildmat.2016.05.080

[34] He, P., Drissi, S., Hu, X., Liu, J., Shi, C., Investigation on the influential mechanism of FA and GGBS on the properties of CO2-cured cement paste, Cem. Concr. Compos., 2023, 142, 105186. doi: https://doi.org/https://doi.org/10.1016/j.cemconcomp.2023.105186

[35] Wu, C.-H., Hong, K.-S., Shih, P.-T., Cheng, T.-W., Lee, W.-H., Using GGBS/FA-based geopolymer on CO2 sequestration and its influence, Constr. Build. Mater., 2025, 494: 143519. doi: https://doi.org/https://doi.org/10.1016/j.conbuildmat.2025.143519

[36] Kim, J.-S., Youm, K. S., Lim, J.-H., Han, T.-S., Effect of carbonation on cement paste microstructure characterized by micro-computed tomography, Constr. Build. Mater., 2020, 263: 120079. doi: https://doi.org/https://doi.org/10.1016/j.conbuildmat.2020.120079

[37] Hwalla, J., Al-Mazrouei, M., Al-Karbi, K., Al-Hebsi, A., Al-Ameri, M., Al-Hadrami, F., et al., Performance of alkali-activated slag concrete masonry blocks subjected to accelerated carbonation curing, Sustainability, 2023, 15(19): 14291. doi: https://doi.org/10.3390/su151914291

[38] Wang, S. Y., McCaslin, E., White, C. E. , Effects of magnesium content and carbonation on the multi-scale pore structure of alkali-activated slags, Cem. Concr. Res., 2020, 130: 105979. doi: https://doi.org/https://doi.org/10.1016/j.cemconres.2020.105979